流體-彈性底床三維音傳模式之建立

計劃編號:NSC 89-2611-E-002-021
執行期限:88年8月1 日至89年7月31日
計劃主持人: 許文翰 國立臺灣大學造船及海洋工程系所 教授

中文摘要

本報告係在建立三維流體-彈性底床內之音傳模式。因單向之音傳特性, 故方程式可以拋物線型化而得以減少計算時間與空間。爲了封閉微分系統, 在水與彈性底床間需給定垂向位移連續及零剪力的條件。所得的數學模型以二階準確的數值方法近似。程式將在水層, 彈性底層及水-彈性底層內作理論之驗證。

英文摘要

We consider in this progress report three-dimensional acoustic wave propagation in fluid-elastic media. These equations are parabolized since only outgoing wave propagation is permitted. This facilitates the analysis, shortens computing time, and reduces disk storage. To couple working equations in fluid and elastic layers, we demand continuity of the normal displacement and normal stress. In addition, physical reasoning requires that shear stresses vanish on the interface for the present analysis, which is formulated under the inviscid flow assumption. We approximate spatial derivatives using the second-order accurate centered scheme. The resulting ordinary differential equation is solved implicitly to render also second-order prediction accuracy in the range direction. With numerical scheme, it is highly desirable to demonstrate the applicability of the code to the individual fluid and elastic layer. We have also verified that the code is applicable to analysis of wave propagation in water and elastic layers, across which there is an interface.

1. Introduction

Early work on the subject of underwater wave propagation dates back to the work of Tappert and McCoy. Wales and McCoy further compared different parabolic theories for modeling the elastic wave propagation in linearly elastic solids. Recently, the fluid-elastic interface problem gradually became the focal research attent on aimed at gaining a better understanding of the underwater acoustic wave propagation. Early development in this area resorted to idealizations in order to make the problem tractable.

Hudson was among the very few authors who considered three-dimensional elastic propagation problems. He derived working equations, written in terms of displacement variab es, but had no attempt to implement them into the numerical computation. More recently, Nagem et al. [1] formulated a set of elastic parabolic equations, paving the way for the later derivation of a three-dimensional coupled fluid-elastic model.

In this report, we develop a space-marching code for equations governing the wave propagation in fluid-elastic medium. It is best hoped that this newly developed computer code provides an alternative to a simulation which has the ability to account for shear wave propagation on the fluid-elastic interface.

2. Mathematical model

In the elastic medium, the stress tensor $\underline{\underline{\tau}}$ can be expressed as a function of the displacement vector $\underline{u}$ and Lame' constants :

$$\underline{\underline{\tau}} = \lambda (\nabla \cdot \underline{u}) \underline{\underline{I}} + \mu \left(\nabla \underline{u} + (\nabla \underline{u})^T \right). \qquad (1)$$

On physical grounds, displacement vectors are continuous across the interface of two media.

Thus, continuity of normal displacement implies that

$$\frac{\partial \phi_1}{\partial z} = \frac{\partial \phi_2}{\partial z} + \frac{\psi_\theta}{r} + \frac{\partial \psi_\theta}{\partial r} - \frac{1}{r}\frac{\partial \psi_r}{\partial \theta}. \quad (2)$$

Another interface condition is derived by considering normal stress components. Physical reasoning dictates continuity of normal stresses between layers of different media:

$$-\rho\,\omega^2\phi_1 = -\lambda\, k_L^2\, \phi_2 + 2\mu\left(\frac{\partial^2\phi_2}{\partial z^2} + \frac{\partial^2\psi_\theta}{\partial r \partial z} + \frac{1}{r}\frac{\partial \psi_\theta}{\partial z} - \frac{1}{r}\frac{\partial^2 \psi_r}{\partial \theta \partial z}\right). \quad (3)$$

Given that the liquid above the interface is inviscid, two shear components tangential to the horizontal interface must vanish. This gives the following interface conditions needed to blend two adjacent layers having different material properties:

$$\frac{2}{r}\frac{\partial^2\phi_2}{\partial\theta\partial z} + \frac{1}{r}\frac{\partial^2\psi_\theta}{\partial r\partial\theta} + \frac{1}{r^2}\frac{\partial\psi_\theta}{\partial\theta} - \frac{1}{r^2}\frac{\partial^2\psi_r}{\partial\theta^2} + \frac{\partial^2\psi_r}{\partial z^2} - \frac{\partial^2\psi_z}{\partial r\partial z} = 0, \quad (4)$$

$$2\frac{\partial^2\phi_2}{\partial r\partial z} + \frac{\partial^2\psi_\theta}{\partial r^2} + \frac{1}{r}\frac{\partial\psi_\theta}{\partial r} - \frac{\psi_\theta}{r^2} \cdots \quad (5)$$

$$\frac{\partial^2\psi_\theta}{\partial z^2} + \frac{1}{r^2}\frac{\partial\psi_r}{\partial\theta} + \frac{1}{r}\frac{\partial^2\psi_z}{\partial z\partial\theta} - \frac{1}{r}\frac{\partial^2\psi_r}{\partial r\partial\theta} = 0, \quad (6)$$

To make the mathematical model well posed for the simulation of acoustic wave propagation in the fluid-elastic environment, it is also important to demand satisfaction of the divergence-free equation on the interface.

3. Space Marching Solution Algorithm

We discretize spatial derivatives with respect to z and θ using the centered scheme to render second-order accuracy. Having discretized equations, the finite difference solutions can then be solved plane-by-plane fashion, starting from the plane $r = r_0$. The analysis is followed by forward marching in the direction of an increasing value of r. Within each marching step Δr, the solutions at the solution plane are computed from

$$\underline{U}^{n+1} = \left(1 + \frac{\Delta r}{2}\underline{\underline{M}}^{n+1/2}\right)\underline{U}^{n+1/2} + \frac{\Delta r}{2}\underline{N}^{n+1/2}. \quad (7)$$

4. Numerical Results

4.1 Validation in the water layer

The problem was chosen to verify the code, which is only applicable to a water layer [2]. In this study, material properties and flow conditions are $H = 100cm$, $\rho_1 = 1g/cm^3$, $\rho_2 = 1.97g/cm^3$, $c_1 = 1507.5m/s$, $\alpha_2 = 1725m/s$, $v_1 = 1500m/s$, $f = 68.03Hz$, $d = 25m$, $\beta_2 = 1530m/s$. In the rectangular physical domain, all the calculations were performed on uniform grids of different grid resolutions. As is evident from Table 1, the computed solutions compare favorably with the corresponding exact solutions.

4.2 Validation in the elastic layer

To verify the applicability of the code to simulation of equations in the elastic bottom, we considered the wave propagation in an unbounded three-dimensional elastic layer. The problem chosen was considered by Lee et al. [3]. In this study, we start the computation at the range value $r = 200m$ and terminate the analysis at the range value $r = 210m$ using a range increment $\Delta r = 1m$. The physical parameters are $\rho = 2400kg/m^3$, $\omega = 1000\pi Hz$ and $\Delta\theta = 1°$. As Table 2 shows, our finite-difference solutions for dependent variables compare well with the analytic solutions.

4.3 Validation in the fluid-elastic layer

Having verified the code in both water and elastic layers, we can proceed to verify the code developed for modeling the fluid-elastic equations used together with the physically sound interface conditions. To our best knowledge, a closed-form solution to this coupled system of equations is still lacking. Therefore, we assign a priori an explicit source vector to make the resulting equation to be amenable to exact solutions given by $\phi\,(r, z, \theta) = r^2z^6\theta^3 + ir^2z^6\theta^3$, where ϕ stands for $r, A^I, B_z^I, B_r^I, B_\theta^I, A, B_z, B_r$, and B_θ.

For completeness, we also plot field variables at $\theta = 5°$ and $z = 50m$ against r. As Figs. 1-5 show, the computed solutions were in good agreement when compared to the analytic data.

5. Concluding Remarks

We have presented a finite difference scheme to solve a parabolized set of fluid-elastic equations. On the horizontal interface, we demand continuity of the normal displacement and the normal stress. In addition, physical reasoning requires that the shear stresses vanish on the interface for the present analysis which is formulated under

the inviscid flow assumption. We discretize spatial derivatives using the second-order centered scheme. The resulting ordinary differential equation has been solved using the implicit Crank-Nicolson marching scheme to render second-order prediction accuracy. Three analytic test problems were chosen to demonstrate the applicability of the code to the fluid, elastic, and fluid-elastic layers.

References

[1] R. J. Nagem, D. Lee, and T. Chen, "Modeling Elastic Wave Propagation in the Ocean Bottom," *J. Math. Modelling and Scientific Computing*, Vol. 2, No. 4, 1995, 1-10.

[2] E. C. Shang and D. Lee, "A Numerical Treatment of the Fluid/Elastic Interface Under Range-dependent Environments," J. Acoust. Soc. Am., Vol. 85, No. 2, 1989, 654-660.

[3] D. Lee, R. J. Nagem and D. C. Resasco, "Numerical Computation of Elastic Wave Equations," J. Computational Acoustics, Vol. 5, No. 2, 1997, 157-176.

Table 1 The computed $L_2-error$ norms for the test problem, given in Section 4.1, at different marching locations.

r	$\Delta = 10m$	$\Delta = 6.25m$	$\Delta = 5m$
1001	3.7511E-05	3.6895E-05	3.6781E-05
1002	7.4993E-05	7.3886E-05	7.3654E-05
1003	1.1256E-04	1.1097E-04	1.1062E-04
1004	1.5011E-04	1.4812E-04	1.4766E-04
1005	1.8774E-04	1.8541E-04	1.8477E-04
1006	2.2556E-04	2.2279E-04	2.2203E-04
1007	2.6346E-04	2.6021E-04	2.5937E-04
1008	3.0140E-04	2.9776E-04	2.9680E-04
1009	3.3947E-04	3.3539E-04	3.3437E-04
1010	3.7765E-04	3.7313E-04	3.7204E-04
1011	4.1615E-04	4.1097E-04	4.0984E-04
1012	4.5514E-04	4.4889E-04	4.4777E-04
1013	4.9477E-04	4.8692E-04	4.8581E-04
1014	5.3528E-04	5.2509E-04	5.2394E-04
1015	5.7683E-04	5.6338E-04	5.6215E-04
1016	6.1951E-04	6.0178E-04	6.0037E-04
1017	6.6338E-04	6.4028E-04	6.3867E-04
1018	7.0845E-04	6.7890E-04	6.7689E-04
1019	7.5476E-04	7.1761E-04	7.1498E-04

Table 2 The computed $L_2 - error$ norms for A, B_r, B_θ, B_z, at different locations r for the test problem given in Section 4.2. The rates of convergence, $\frac{\log(\frac{err_1}{err_2})}{\log(\frac{\Delta z_1}{\Delta z_2})}$, are also computed.

A			
r	$\Delta = 5m$	$\Delta = 4m$	*Rate*
201	5.8624E-10	4.6002E-10	1.0866E+00
202	1.1415E-09	9.1712E-10	9.8113E-01
203	1.6692E-09	1.3737E-09	8.7307E-01
204	2.1740E-09	1.8322E-09	7.6669E-01
205	2.6621E-09	2.2942E-09	6.6648E-01
206	3.1403E-09	2.7609E-09	5.7697E-01
207	3.6163E-09	3.2329E-09	5.0215E-01
208	4.0973E-09	3.7098E-09	4.4519E-01
209	4.5902E-09	4.1905E-09	4.0825E-01
210	5.1005E-09	4.6730E-09	3.9230E-01

B_r			
r	$\Delta = 5m$	$\Delta = 4m$	*Rate*
201	3.9480E-08	2.7723E-08	1.5843E+00
202	7.9668E-08	5.4048E-08	1.7387E+00
203	1.1982E-07	7.9425E-08	1.8428E+00
204	1.5910E-07	1.0455E-07	1.8814E+00
205	1.9661E-07	1.3021E-07	1.8465E+00
206	2.3156E-07	1.5709E-07	1.7389E+00
207	2.6326E-07	1.8554E-07	1.5679E+00
208	2.9123E-07	2.1556E-07	1.3483E+00
209	3.1521E-07	2.4672E-07	1.0979E+00
210	3.3516E-07	2.7824E-07	8.3407E-01

B_θ			
r	$\Delta = 5m$	$\Delta = 4m$	*Rate*
201	2.8169E-09	1.9465E-09	1.6563E+00
202	5.4409E-09	3.6959E-09	1.7330E+00
203	8.0940E-09	5.4037E-09	1.8106E+00
204	1.0682E-08	7.0988E-09	1.8315E+00
205	1.3141E-08	8.8258E-09	1.7840E+00
206	1.5416E-08	1.0622E-08	1.6693E+00
207	1.7465E-08	1.2506E-08	1.4966E+00
208	1.9257E-08	1.4471E-08	1.2804E+00
209	2.0780E-08	1.6485E-08	1.0375E+00
210	2.2035E-08	1.8497E-08	7.8430E-01

B_z			
r	$\Delta = 5m$	$\Delta = 4m$	*Rate*
201	4.3425E-10	2.9452E-10	1.7399E+00
202	8.7138E-10	5.8465E-10	1.7883E+00
203	1.3047E-09	8.7533E-10	1.7886E+00
204	1.7265E-09	1.1722E-09	1.7354E+00
205	2.1292E-09	1.4802E-09	1.6290E+00
206	2.5053E-09	1.8024E-09	1.4755E+00
207	2.8488E-09	2.1387E-09	1.2848E+00
208	3.1553E-09	2.4857E-09	1.0689E+00
209	3.4223E-09	2.8370E-09	8.4053E-01
210	3.6493E-09	3.1838E-09	6.1147E-01

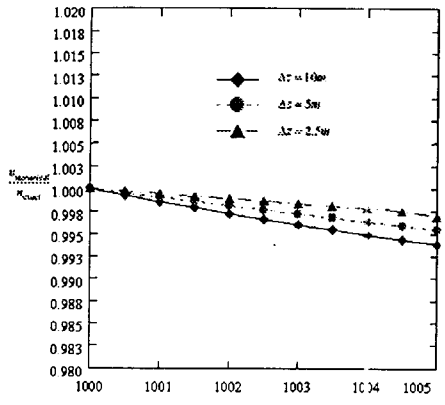

Figure 1: The computed ratios between the numerical and exact solutions for the field variable u against r for the problem considered in Section 4.3

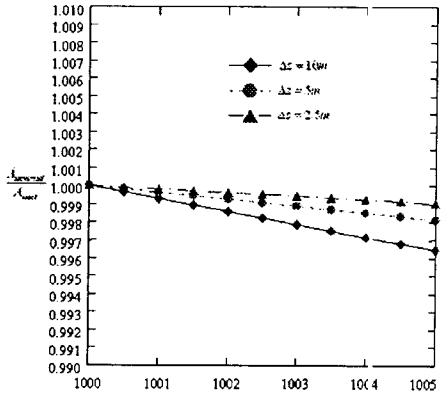

Figure 2: The computed ratios between the numerical and exact solutions for the field variable A against r for the problem considered in Section 4.3.

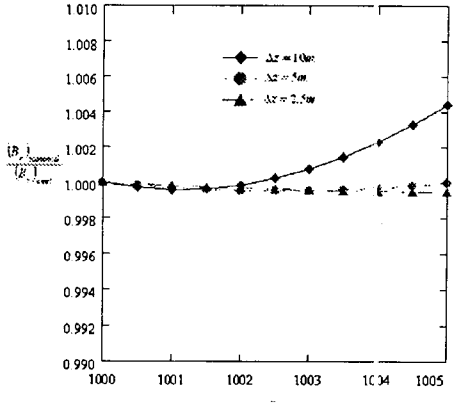

Figure 3: The computed ratios between the numerical and exact solutions for the field variable B_r against r for the problem considered in Section 4.3.

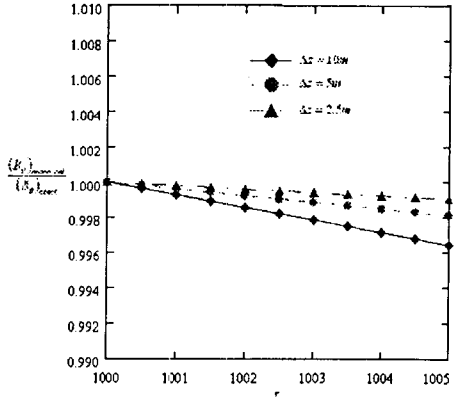

Figure 4: The computed ratios between the numerical and exact solutions for the field variable B_θ against r for the problem considered in Section 4.3.

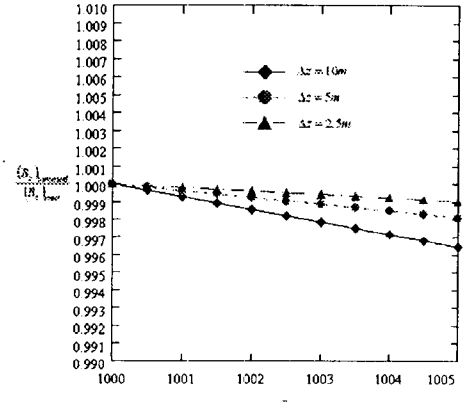

Figure 5: The computed ratios between the numerical and exact solutions for the field variable B_z against r for the problem considered in Section 4.3.